Title: The role of time-varying viral shedding in modeling environmental surveillance for public health: revisiting the 2013 poliovirus outbreak in Israel

Authors: Andrew F. Brouwer[1], Marisa C. Eisenberg[1], Lester M. Shulman[2,3], Michael Famulare[4], James S. Koopman[1], Steve J. Kroiss[4], Musa Hindiyeh[2], Yossi Manor[2], Itamar Grotto[5,6], Joseph N.S. Eisenberg[1]

[1]Department of Epidemiology, University of Michigan, Ann Arbor, Michigan, United States

[2]Central Virology Laboratory, Chaim Sheba Medical Center, Tel-Hashomer, Israel

[3]School of Public Health, Sackler Faculty of Medicine, Tel Aviv University, Tel Aviv, Israel

[4]Institute for Disease Modeling, Bellevue, Washington, United States

[5]Ministry of Health, Jerusalem, Israel

[6]Department of Public Health, Faculty of Health Sciences, Ben-Gurion University of the Negev, Beer Sheva, Israel

Corresponding authors: Andrew F. Brouwer, 1415 Washington Heights, Department of Epidemiology, University of Michigan, Ann Arbor, MI 48109; brouweaf@umich.edu; Joseph N. S, Eisenberg, 1415 Washington Heights, Department of Epidemiology, University of Michigan, Ann Arbor, MI 48109; jnse@umich.edu

Declarations of conflicts of interest: The authors declare they have nothing to disclose.

Abstract

Environmental pathogen surveillance is a sensitive tool that can detect early-stage outbreaks, and it is being used track poliovirus and other pathogens. However, interpretation of longitudinal environmental surveillance signals is difficult because the relationship between infection incidence and viral load in wastewater depends on time-varying shedding intensity. We developed a mathematical model of time-varying poliovirus shedding intensity consistent with expert opinion across a range of immunization states. Incorporating this shedding model into an infectious disease transmission model, we analyzed quantitative, PCR data from seven sites during the 2013 Israeli poliovirus outbreak. Compared to a constant shedding model, our time-varying shedding model estimated a slower peak (4 weeks later), with more of the population reached by a vaccination campaign before infection and a lower cumulative incidence. We also estimated the population shed virus for an average of 29 days (95% CI 28–31), longer than expert opinion had suggested for a population that was purported to have received three or more inactivated polio vaccine (IPV) doses. One explanation is that IPV may not substantially affect shedding duration. Using realistic models of time-varying shedding coupled with longitudinal environmental surveillance may improve our understanding of outbreak dynamics of poliovirus, SARS-CoV-2, or other pathogens.

Introduction

Environmental pathogen surveillance—the systematic testing of environmental samples for the presence or concentration of pathogens—is increasingly recognized as a sensitive means of disease surveillance, thus allowing for better disease control. New molecular tools are being developed to detect a wide variety of pathogens (e.g., enteric pathogens, respiratory pathogens (including SARS-CoV-2)) in a range of environmental contexts (e.g., wastewater, aerosols, wildlife feces) [1–11]. The global pandemic of COVID-19 has further accelerated interest in environmental surveillance research, as well as the need for—and the challenges and ethical questions associated with—developing robust environmental surveillance methods to inform real-time public health decision-making [12–17].

One important use of environmental surveillance is as an early warning indicator of community transmission. The potential for environmental surveillance to detect transmission earlier than case surveillance depends on the timing of shedding relative to symptom onset as well as the relative clinical and environmental testing capacity and reporting infrastructure [18]. The use of environmental surveillance as an early warning sign is exemplified in the context of polio, where, for example, it was used to identify extensive poliovirus transmission in southern Israel in 2013 in the absence of any cases of acute flaccid paralysis (AFP) [19]. AFP is the standard epidemiological surveillance mechanism for identifying active transmission, but AFP only occurs in 1:100 to 1:2000 infections and can be further blunted if part of the population has received inactivate polio vaccine (IPV), which prevents AFP but not infection. Reliance on AFP alone can result in delayed detection of an outbreak, allowing poliovirus to circulate and infect a large number of people before a case of AFP is detected. Poliovirus transmission without associated cases of AFP is called silent circulation [9].

Beyond providing early warning through pathogen detection, environmental surveillance has the potential to inform population disease incidence trends, providing valuable information on outbreak severity and dynamics [20]. Basic analytic tools for interpreting presence/absence and quantitative environmental surveillance are now being developed to provide public health relevant metrics [20–23]. However, more work is needed to understand how an environmental signal translates to the number of people or fraction of the population shedding. Previous work, including our own, has assumed constant shedding over the infectious period [20, 21], but pathogen shedding intensity can vary by several orders of magnitude over the course of infection [24, 25]. Explicitly accounting for both time-varying shedding

intensity and the population distribution of shedding duration is essential to using environmental surveillance to accurately inform the epidemiology of outbreaks of these pathogens.

Here, we developed models of time-varying shedding intensity informed by an expert opinion synthesis of existing data [24] and integrated them into our previously developed transmission modeling framework that transformed environmental surveillance data into estimates of polio incidence patterns. We used this updated framework to analyze the quantitative environmental surveillance data from seven sites in the Negev region of southern Israel during the 2013 silent polio outbreak to re-examine the epidemiology of the regional epidemic. We explored two questions that can only be answered with a time-varying framework, namely 1) How do estimates of outbreak characteristics such as cumulative incidence and peak time change when incorporating time-varying shedding; and 2) What duration of shedding is most consistent with the environmental surveillance patterns, and what does that suggest about the immunity of the at-risk population? We also discuss the implications of our results for understanding the spatial pattern of disease spread and health disparities related to ethnicity. These issues may impact the surveillance and management of future poliovirus outbreaks.

Data

Environmental surveillance

We used environmental surveillance samples collected between March and December 2013 from the Ar'ara, Be'er Sheva, Rahat, and Shoket wastewater treatment plants and from trunk lines in Arad (Kseife branch), Ayalon (Lod branch), and Tel Sheva. Sampling rates varied over the time period but were approximately weekly starting in May. An automatic, in-line sampler collected and pooled samples over a 24-hour period [9]. The first WPV1-positive samples were collected on March 11th, 2013 in Be'er Sheva and Rahat. Wild poliovirus type 1 (WPV1), oral poliovirus type 1 (OPV1), and oral poliovirus type 3 (OPV3) were separately quantified. We treated multiple data points from the same location and time as distinct. The datasets supporting this article have been uploaded as part of the supplementary material.

Connecting PCR cycle threshold to pathogen concentration

The laboratory analysis of the wastewater samples reported results in terms of quantitative reverse transcriptase polymerase chain reaction (qRT-PCR) cycle threshold. Briefly, qRT-PCR targets a specific viral RNA area of interest and transcribes the RNA into DNA. That DNA sequence is then amplified in each PCR

cycle; the number of amplification cycles needed for the number of copies of the targeted DNA sequence to reach a threshold number τ (set by the test operator above the background noise) provides a means to quantify concentration. The number of doubling cycles, denoted y, needed for a sample to achieve the threshold is called the cycle threshold (Ct). A higher Ct value indicates a lower concentration of virus in the original sample. The Ct value y is mathematically related to the concentration of poliovirus W in wastewater samples through the standard PCR amplification equation $\tau = W \cdot (1 + \epsilon)^y$, where τ is the threshold copy number (essentially, a reference concentration with the same units as W) and is the reaction efficiency (typically 90–110% [26]). In the absence of experimental information, we assume $\epsilon = 1$, so that $y = \log_2(\tau/W)$. The laboratory method used to obtain Ct values for the 2013 outbreak has been described elsewhere [27–30]. The limit of detection in this assay was on the order of 40 cycles, but the experiments were run to 60 cycles to distinguish between negative samples and samples near the limit of detection [27].

Vaccination campaigns

Israel conducted two supplementary bivalent oral polio vaccine (bOPV, which contains OPV1 and OPV3 Sabin strains) campaigns during the epidemic. The first began on August 5, 2013, lasted one month, and achieved 90% coverage in children under ten; the second began on October 7, 2013, lasted about 10 days, and achieved 53% coverage [31]. We used vaccine time-series data to estimate a constant average per capita vaccination rate ϕ =0.074/day during both campaigns, with no bOPV vaccination between the campaigns. We assumed that the vaccination take rate was 80% [32].

Mathematical Modeling

The overall goal of this analysis was to understand the epidemiology of the poliovirus outbreak in 2013 in southern Israel. Because our data are wastewater surveillance concentrations, accounting for time-varying shedding is essential to be able to connect the wastewater signals to population-level epidemic curves. We needed to account not only for duration of shedding but also its relative magnitude over the shedding period. To do this, we used a two-part approach. First, we developed a model of time-varying shedding and calibrated it to an expert synthesis of data. Second, we used the calibrated shedding model within an infectious disease transmission model. Below, we outline the approach for each of these models.

Shedding model

While some previous models have explored time-varying infectiousness (e.g., [33, 34]), few models have attempted to describe time-varying shedding. One notable exception is Famulare et al. [25], who fit log-normal survival models to poliovirus shedding duration by strain and immunization history. Because survival models cannot be directly incorporated into compartmental, ordinary differential equation infectious disease transmission models, we took a different approach here. We developed a time-varying shedding model that uses a distributed-delay framework (i.e., gamma-distributed residence times) [35–37], similar to some approaches for time-varying infectiousness [33]. Distributed delays are often used in infectious disease transmission models to better reproduce observed distributions of the latent or infectious period. Specifically, our shedding model describes infected individuals as being in states exhibiting no shedding, low levels of shedding, or high levels of shedding. Each of these states is described by a series of compartments, each with a rate parameter summarizing the rate of leaving the compartment and an average shedding concentration. Broadly, our shedding model captures a latent period, in which an individual does not shed, followed by short-term low-, high-, and low-shedding states, each modeled with one or more compartments, followed by a longer-term low-shedding state modeled with a single compartment to capture heterogeneity in long-term shedding (figure 1). Our shedding model was designed, on the one hand, to be parsimonious with respect to the number of compartments and parameters and, on the other hand, to be flexible enough to capture patterns for a variety of prior immunization histories. These models are meant to capture broad population averages rather than individual trajectories.

We calibrated our models by hand to a data set of previously published expert opinion of shedding duration and shedding concentration trajectories across a variety of prior immunization histories. The expert elicitation solicited the opinion of nine experts on a wide range of topics related to the implications of poliovirus immunity states [24]. Most relevant to this study, each expert indicated the fraction of the population shedding fecally (and the concentration shed if shedding) for the first seven days after exposure and every 7 days after for a few different polio immunity states ranging from fully susceptible to immunization with both IPV and OPV. As calibration tests for our model, we selected trajectories defined by the mean expert opinion for three immunity states, namely fully susceptible (no immunization), those having 3 or more doses of IPV, and those having both IPV and OPV. We used expert opinion data here, which represent a synthesis and extrapolation of existing experimental data, because

the underlying experimental data do not fully cover the range of relevant scenarios. While we used the expert opinion data to calibrate the general shape and timing of the longitudinal dynamics, we do not directly use the experts' estimates of the magnitudes of viral shedding in our analysis of the wastewater data. As we discuss in greater detail below, the shedding magnitudes are not individually identifiable because the virus is diluted in an unknown volume of wastewater, but the ratio of the high-shedding to low-shedding concentration is identifiable, and we estimate it from the surveillance data.

Infectious disease transmission model

We modeled an at-risk population of unknown size composed of children under 10 years old (as well as unvaccinated immigrants and any adults whose immunity may have waned). IPV is part of the pediatric vaccination program in Israel, with 90–95% of children in the area receiving at least 3 doses [38], but OPV was not used in Israel for pediatric vaccination between 2005 and the 2013 outbreak in order to minimize the risk of cVDPVs [19]. We modified our previously developed SLIR-type model [20] to incorporate our variable shedding model and account for WPV1 infection, vaccination with bOPV in response to the outbreak, and subsequent transmission of OPV1 and OPV3 (figure 2 and table 1). This model tracks the fraction of the population that is susceptible S, latent L, infectious I, recovered R for poliovirus type 1 and 3 independently, distinguishing between infections of wild and vaccine types. That is, individuals may be latent, infectious, or recovered with either WPV1 (subscript $w1$) or OPV1 (subscript $o1$) strains but not both, and we track OPV3 (subscript $o3$) disease status independently of WPV1 and OPV1 disease status. We also track the pathogen concentration in wastewater W for each of WPV1, OPV1, and OPV3. As in [20], we estimate the transmission rate for WPV1 (β) but fix the ratio ρ of transmission rates for OPV1 to WPV1 and OPV3 to WPV1 to 0.37 and 0.20 respectively [33]. Model equations are provided in the supplementary material.

We modeled the latent and infectious states using a shedding model; the specific number and parameterization of the subcompartments was determined by the model calibration, which we describe below in the Results. We designated the latent stage transition rate in the ith latent compartment as σ_i and the infectious stage transition rate in the ith infectious compartment as γ_i. We used the same shedding model for wild and OPV type virus, except that we allowed the shedding concentrations to differ. The specific magnitudes of shedding in the low- and high-shedding states cannot be estimated because the volume of wastewater in which the virus is diluted is unknown. Instead, we estimated the ratio λ of

shedding concentration in the low-shedding compartments to that in the high-shedding compartments; we estimated this ratio for the OPV types (λ_o) separately from the wild type (λ_w). Based on the calibration results, discussed below, we assumed that only the high-shedding infectious individuals transmit infection. While not strictly true from an individual perspective, that assumption is consistent with the time-varying shedding model when viewed from a population-average perspective.

Because each site will vary in wastewater volume, flow rate, etc., we cannot directly compare the PCR data for each strain across the seven sites. From the data alone, we cannot distinguish, for example, whether the virus is decaying quickly in a large volume or slowly in a small volume. To account for these kinds of trade-offs, we defined a site-specific scaling parameter κ for each site j and each virus type k. This parameter summarizes several mechanistic parameters that cannot be individually determined from the data. Specifically, $\kappa_{k,j} = \xi_{k,j}\tau/\alpha_{k,j}$, where $\alpha_{k,j}$ is the high-level shedding rate (accounting for site-specific wastewater volume), $\xi_{k,j}$ the removal/decay rate of poliovirus, and τ is the PCR threshold parameter, which could in general be known from the lab is treated as unknown here. Note that between-lab differences in sample handling would also need to be accounted for here when using data from multiple labs. These scaling parameter combinations $\kappa_{k,j}$ can be estimated from the data even though their constituent parameters cannot [20].

As a default, we made the biologically plausible assumption that the ratio of shedding rates of WPV1 to OPV1 to OPV3 do not vary across surveillance sites but that each surveillance site may have different dilution factors (accounted for in each α and thus κ). Preliminary analysis indicated that this assumption was valid for the majority of the sites but was violated at three of them (Ayalon, Be'er Sheva, and Shoket). Because each of these three communities have both Bedouin and Jewish populations, while the other sites are primarily Bedouin, we hypothesized that the ratio of WPV to OPV in wastewater could be altered if OPV were given to a population of children who were not at-risk of WPV infection because we would then see more OPV in the wastewater relative to what we would expect given the amount of WPV observed. This situation could potentially arise if there was low contact between children of different ethnicities. We modeled these three sites accordingly (details in the supplementary material), estimating the relative size of this not-at-risk population η for each of the three sites separately.

Integration of shedding model into the infectious disease model framework

We expected that the immunity of the target population in Israel prior to the supplemental bOPV immunization campaign to be somewhere between no immunization and 3+ doses of IPV. Accordingly, we implemented the shedding model in the infectious disease transmission by fixing the number and duration of the latent and infectious compartments to that of the no immunization history model (which were the same as those of the 3+ doses of IPV model, see Results), with the exception of the duration of the long-term, low-shedding compartment, which we estimated. The estimated duration of this long-term compartment allowed us to make inferences about prior immunization in the population.

To account for time-varying infectiousness through the relative infectiousness of the high and low shedding concentrations, we modeled the expert opinion data on the relationship between shedding concentration and infectiousness using log-normal distributions (figure S1). Based on our model calibration results and the expert opinion, we estimated that the high-shedding concentration is 5–10 times as infectious as the low-shedding concentration. This estimate serves as the justification for our simplifying assumption that only individuals in the high-shedding state transmit infections in our infectious disease model. Note, however, that modeling of other pathogens and contexts will likely require alternative assumptions regarding the relative infectiousness of low- and high-shedding states.

As a comparison for the variable shedding model, we also adapted our previous constant shedding model [20] to fit the multisite data. This model uses a single compartment for each of the latent and infectious classes and assumes that the infectious period is the same as the shedding period. More details are given in the supplementary material, including a comparison of the population-average force of infection over the infectious period (figure S2).

Simulation and parameter estimation

We fit the model to the WPV1, OPV1, and OPV3 PCR CT data as in [20]. At time $t = 0$ (March 11, 2013), we assumed no bOPV vaccination (i.e. $\phi = 0$) and no recovered people in the modeled population. We modeled the vaccination rate as a fixed, non-zero constant ϕ during the two vaccination campaigns, which began August 5 and October 7, 2013 and were modeled as lasting 31 and 10 days, respectively; the vaccination rate was zero at all other times. We estimated the initial condition (details given in

supplementary material). All simulations and analyses were done in R (v.3.4.1; R Foundation for Statistical Computing; Vienna, Austria). We used deSolve for ODE model simulation and the David–Fletcher–Powell algorithm in the Bhat package for maximum likelihood estimation [39, 40].

As described above, because the shedding concentrations $\alpha_{k,j}$, removal rates $\xi_{k,j}$, and qRT-PCR threshold concentration τ cannot be individually determined from the data alone, we estimate site-specific scaling parameters $\kappa_{k,j} = \xi_{k,j}\tau/\alpha_{k,j}$ instead. Similarly, the concentration of poliovirus W_k in wastewater can only be determined up to a constant [20], so we instead estimate a scaled concentration $\overline{W}_{k,j} = \xi_{k,j}W_{k,j}/\alpha_{k,j}$, which is approximately equal to I_k for fast $\xi_{k,j}$ (see [20] for additional technical details). Accordingly, we transform our measurement equations from $y_{k,j} = \log_2(\tau/W_{k,j})$ to $y_{k,j} = \log_2(\tau/I_{k,j})$ for each of WPV1, OPV1, and OPV3. All seven sites were simultaneously simulated. We used a sum of absolute differences (L^1) approach on the Ct scale, heuristically resulting in the median trajectory instead of the mean trajectory. This eliminates the sensitivity of the results to the choice of 60 as the "absence of poliovirus" value. This approach is equivalent to maximum likelihood estimation under the assumption that errors are Laplace distributed. We minimize the negative log-likelihood, $NLL(\boldsymbol{\theta}) = \left(\sqrt{2}/\varsigma\right)\sum_i |y_i - \hat{y}_i(\boldsymbol{\theta})|$, where $\{y_i\}$ the Ct data, ς is the variance of the error distribution of the data, $\{\hat{y}_i\}$ are the modeled Ct values, and $\boldsymbol{\theta}$ is the vector of model parameters (listed in table 2). We set ς=0.98 based on data analysis of the multiple qPCR tests of wastewater samples collected on certain days.

Likelihood-based 95% confidence intervals for parameter estimates were determined by parameter profile likelihoods [41]. These profile likelihoods are transects through the 95% confidence region of parameter space. We simulated trajectories for each parameter vector in each profile and estimated the 95% confidence intervals for the maximum likelihood trajectory to be the maximum and minimum at each time point in this set of simulated trajectories.

Results

Time-varying shedding model calibration

The mean expert opinion provided by [24] and our calibrated shedding models fits are shown in figure 3. Details of the parameterizations for the trajectories of each immunization history are provided in the supplementary material. The mean WPV1 shedding duration for each immunization state was 28 days for

the fully susceptible, 18 days for those with 3+ doses of IPV, and only 10 days for those with both OPV and IPV.

Estimated parameters

Estimates of the infectious disease and shedding model parameters are given in table 2. We estimated that the average shedding duration was 29.4 days (95% CI 27.7–31.3). The site-specific scaling parameters $\kappa_{k,j}$, which account for differences in typical wastewater volume and flow between sites, varied by almost two orders of magnitude. These large differences are not surprising, given likely differences in sewer parameters, greywater volumes, etc., and reflect systematic differences in the qRT-PCR Ct values themselves; e.g., the qRT-PCR Ct values in Arad were overall lower than those in Ayalon, indicating a consistently greater concentration of virus in the samples across the outbreak. We estimated that WPV1 was shed at concentrations approximately 10.0 (95% CI: 7.8–15.6) times those of OPV1 and 3.7 (95%CI 2.7–5.1) times those of OPV3. The estimated WPV1:OPV1 ratio is within an order of magnitude of the ratio estimated from empirical concentrations of WPV1 (2×10^6 PFU/g) and OPV1 (3×10^4 PFU/g) in children's stool [42]. These modeled ratios were consistent for four of the sites, namely Ar'ara, Arad, Rahat, and Tel Sheva. Data from the other three sites violated this assumption (Ayalon Lod, Be'er Sheva, Shoket), and we estimated site-specific relative sizes of vaccinated but not-at-risk populations to account for the relatively greater comparative concentration of OPV in their wastewater, as discussed in the Methods.

Epidemic dynamics

From the best-fit parameters, we estimate that the epidemic peaked mid-July (maximum-likelihood estimate: July 14; 95% CI: July 4 – August 4) (figure 4a) and that R_0 was 1.48 (95% CI: 1.39– 1.55). We estimate that the epidemic infected 50.7% (95% CI: 37.8–57.9%) of the at-risk population and that the vaccination campaign averted 10.9% (95% CI: 5.5–24.5%) of infections. Relative to the constant shedding model, the variable shedding model predicts a later (approximately 4 weeks later) and larger epidemic peak (figure 4b). The constant shedding model peaks earlier and predicts a larger cumulative incidence (74.2% compared to 50.7%) and smaller fraction of the population vaccinated prior to possible infection (24.0% compared to 45.9%) than the variable shedding model. It may be initially counterintuitive that the variable shedding model has a larger epidemic peak and area under the curve but a smaller cumulative incidence. This result is driven by differences in the infectious and shedding periods for the two models.

The constant shedding model represents a shedding period of 13 days; individuals are fully infectious for that period. In the variable shedding model, on the other hand, individuals shed for 29 days but are effectively infectious and shedding high amounts of virus for only 3 days (and shedding low amounts of virus for the rest of the period). A comparison of the force of infection and shedding magnitude as a function of time since infection between the variable and constant shedding models is given in the supplementary material (figure S2). Thus, the constant shedding model, with the longer infectious period and larger R_0 (1.94), has faster epidemic growth and cumulative incidence, but it has a lower peak because it has a shorter shedding duration. Overall, the variable shedding model is better able to capture the dynamics of the longitudinal environmental surveillance data. Specifically, the variable shedding model achieved an Akaike Information Criterion (AIC) of -76.4, indicating that it offers a substantial improvement to the model fit with only two additional parameters (a comparative plot of the fits to the PCR CT data is provided in figure S3).

We plot the model trajectory with the qRT-PCR Ct data for each site and each strain in figure 5a, b, and c. In these plots, we scaled each site's qRT-PCR data by $\log_2$ of their respective site-specific scaling parameter κ, so that they can be compared to a common model trajectory (see supplementary material). These plots indicate that the data are consistent with the assumption that the outbreak proceeded essentially in parallel throughout southern Israel. Ayalon Lod, Be'er Sheva, and Shoket are censored in the figure 5b and c because those sites are modeled with an additional population receiving OPV; because the OPV dynamics in the wastewater of these sites are different from the other four, they are not directly comparable to a common model. Model trajectories fit to the unscaled qRT-PCR Ct data from each site are shown in figure S4. Although the sites vary in terms of overall data coverage and, to some degree, the variance in the data, the model is a reasonable fit in each case.

Discussion

Environmental pathogen surveillance has the potential to transform how we understand and analyze disease outbreaks. To reach this potential, laboratory techniques, sampling coverage, and analytical methodology all need to be further developed. Here, we demonstrated that leveraging enhanced SIR-type transmission models to include time-varying shedding dynamics improves our interpretation of the environmental surveillance data. This enhancement lets us reinterpret the dynamics of the epidemic and estimate shedding duration, challenging prior assumptions about IPV. Additionally, our analysis,

consistent with previous work [28], suggests the local outbreak dynamics in the cities across the region were largely in parallel (i.e., all occurred at the same time) rather than sequential and spatial (as would have been the case if infection were seeded in one city and spread outward).

Our augmented models allow us to revisit previous estimates of the 2013 Israeli poliovirus outbreak timing and cumulative incidence. In particular, the model with time-varying shedding estimated the outbreak peaked about 4 weeks later (mid-July) compared to the model with constant shedding (mid-June). Accordingly, we estimate that approximately 50% of the at-risk population was infected prior to vaccination and 50% vaccinated before possible infection, rather than the 75%–25% split estimated by the constant shedding model. For comparison, the results of our previous analysis using a constant shedding model on the data from Rahat alone falls somewhere between these two models, with about 60% incidence and a late June peak. These results also underscore the fact that adding variation to non-linear systems can have unexpected or counterintuitive effects.

Based on OPV and IPV history in Israel, we expected the estimated shedding duration to be consistent with what experts have estimated for people with three or more doses of IPV, i.e., shedding for about 18–20 days [24, 25, 33]. In 2005, Israel discontinued use of OPV, which contains a live-attenuated virus that provides gut immunity [19]. Accordingly, the at-risk population for this outbreak is likely largely children under the age of 10 (who would not have received OPV) and older people whose immunity has waned. These children should have received up to five doses of IPV at ages 2, 4, 6, and 12 months and 7 years [38]. (IPV provides humoral immunity, preventing paralysis but not transmission). In this analysis, we estimated a shedding duration of 29.4 days (95% CI: 27.7–31.3), more consistent with estimates for fully susceptible people, which range from 28 to more than 40 days [24, 25, 33], than for those with several doses of IPV. Our finding that the data are consistent with shedding durations longer than expected given the presumed immunity status could be explained by low vaccination coverage or vaccine take rates in the Bedouin communities, many of which are unrecognized. However, Israel Ministry of Health vaccination records indicate at least 90% IPV coverage in these communities, which is consistent with the absence of AFP despite high estimated cumulative incidence. Nevertheless, even with high coverage of IPV, the detected viral signals could be driven by a smaller fraction of the population that was unvaccinated, leading us to estimate a shedding duration consistent with fully susceptible individuals. An alternative explanation for our results is that IPV may not confer as much reduction in the shedding period, suggesting that the expert opinion may be overestimating the impact of IPV on shedding duration.

Most studies that have shown an impact of IPV on shedding duration were from the 1960s and may have been biased by unaccounted-for boosting from residual circulation [25]. More recent studies show no impact on IPV on shedding [43, 44] and other studies have found no correlates of mucosal immunity in populations that have had only IPV [45]. Moreover, although ensemble opinion tends to be more accurate than individual opinion, we recognize the substantial variation in expert opinion. We also acknowledge that many of the studies underlying the expert opinion come from challenge studies in artificial environments that may not exactly reflect real-world conditions. Our results could be caused by model misspecification, as the duration estimates were not strongly robust to the choice of shedding model. Misspecification could also occur if there was unaccounted-for time-varying transmission. Finally, it may also be the case that our results (based on PCR analysis) are in fact consistent with expert opinion (based on cultures), with the excess shedding period in our model capturing the shedding of non-culturable but PCR-detectable virus. Ultimately, more work is needed to better understand poliovirus shedding dynamics for different immunity states. A possible next step would be to use shedding models calibrated directly to available or newly measured shedding data. Our approach to time-varying infectiousness was also simplistic (assuming low-shedders were not infectious); other models have explored gradients in infectiousness over subsequent compartments [33], leading to different assumptions about the force of infection over the shedding period (figure S2). Having both wastewater and infection data in future studies could help resolve the relationship between time-varying shedding and infectiousness.

Although we expected to see spatiotemporal dynamics in these data, the outbreak appears to have occurred approximately simultaneously across the southern Israel, i.e., the dynamic patterns in environmental surveillance are remarkably similar across the sites (figure 5a). The synchronized progression of outbreaks, which suggests rapid seeding of outbreaks across the region, runs counter to one hypothesis that poliovirus transmission outside of focal subpopulations is rare. It may be the case instead that exportation from epicenters is common but rarely sparks outbreaks due to sufficient population immunity from OPV vaccination in more commonly exposed settings. There is some evidence for this explanation in the larger regional picture for this outbreak. The same WPV1 strain responsible for the Israeli outbreak was previously detected in wastewater in Egypt [46] and was subsequently detected by environmental surveillance in the West Bank and Gaza [47] and by AFP surveillance in Syria [48]. Transmission was sustained in Syria, where OPV vaccination was disrupted by civil war [48], and Israel, where OPV use had been suspended in favor of IPV. But, transmission was not sustained in Egypt, the

West Bank, and Gaza, where OPV was still part of vaccination programs. This picture is somewhat complicated by the outbreak in Somalia [49], which had sustained transmission despite exclusive use of OPV, though the outbreak could also be explained by the low historical vaccine coverage there [50]. In this analysis, however, we recognize that the lack of evidence for spatial spread may instead be a lack of the right data. Specifically, we have comparably little data toward the beginning of the outbreak, prior to the expansion of environmental surveillance [9]. Our inferences are, therefore, much stronger regarding the decay of the outbreak rather than its beginning. The existing longitudinal, frequently sampled, and quantitative data from several sites across the region is extremely valuable, but there is no data from unplanned Bedouin communities, which have poor sanitation infrastructure and may have been early transmission hot spots. As we continue to pursue polio eradication in Pakistan and Afghanistan, it is paramount that we have comprehensive, granular environmental surveillance coverage, even in locations where poliovirus is not expected.

Our estimates of the relative shedding rates of WPV1, OPV1, and OPV3 were consistent across the majority of sites, as one would expect if infection biology were consistent across sites. However, three sites deviated from this pattern; Ayalon, Be'er Sheva, and Shoket each had higher concentrations of bOPV in their wastewater than would have been expected given the concentrations of WPV1. Because these three sites were the only ones sampled with substantial Jewish populations, one explanation of these results is that the Jewish children received bOPV but had little contact with the Bedouin under-10 population in the region. While this hypothesis is not a definitive explanation, an epidemiological separation between the communities is supported by observations from the stool survey conducted during the epidemic, which found WPV1 shedding in 5.4% of Bedouin children and 0.6% of Jewish children [42]. It is also supported by the initial, exploratory phase of environmental surveillance in May 2013 (used to decide which sites to continue to monitor weekly), which found differences in detections between neighborhood-level trunk lines within communities. For example, the Arad–Arad trunk line (Jewish neighborhood) was negative while the Arad–Kseife trunk line (Bedouin neighborhood) was positive. Similarly, while the Be'er Sheva (a mixed ethnicity city) treatment plant was positive, the Be'er Sheva North trunk line (Jewish neighborhood) was negative. While social separation is one explanation for differential transmission potential, other differences in population or contact structure (such as population density, family size, and frequency and type of typical physical contact) may also be relevant. This outbreak highlights the potential for racial and ethnic assortativity and the larger geopolitical context

to complicate outbreak intervention and global polio eradication more generally. It also underscores the benefit of using a mathematical model to analyze surveillance data, as we were able to identify these nuanced differences in the dynamics across the sites that might have otherwise gone unnoticed when looking at the PCR data alone.

Eradication efforts for polio have benefited greatly from the expansion of environmental surveillance in the countries with endemic polio infections [22, 51–54]. Beyond polio, control efforts for a wide range of pathogens could benefit from systematic environmental surveillance, which promises to be a cost-effective supplement to active case surveillance, even or especially in low-resource settings [55]. The COVID-19 pandemic has greatly accelerated interest in detecting SARS-CoV-2 and other pathogens in wastewater, which has led to an expansion of collection infrastructure and refinement of laboratory methods [12–14, 56]. Detection and quantification tools are being developed, particularly for enteric and respiratory pathogens, for a range of environmental contexts (e.g., wastewater, aerosols, wildlife feces) [1–14]. An additional benefit of this recent move toward using environmental data to understand the epidemiology of infectious diseases is that it highlights areas of the science of infection and pathogen shedding dynamics that we do not fully understand (e.g., does SARS-CoV-2 fecal shedding differ between variants?). More broadly, our work reflects increasing interest in leveraging population-level aggregates of quantitative pathogen data [57], such as in recent work modeling qRT-PCR Ct values of viral loads from a cross-sectional sample of the population [58].

We would ideally be able to estimate the number of infected individuals based on the pathogen concentration in a single grab sample of wastewater. It will be challenging to do so with any certainty from an isolated sample, but it could be accomplished in the context of systematic environmental surveillance by coupling our model-based approach presented here with both reliable estimates of shedding concentration over time and a way to estimate sewage dilution volume. Both estimates may vary geographically. A promising indirect approach to account for sewage dilution volume is to use a molecular marker correlated with wastewater strength as a normalizing factor for the pathogen concentration [56]. Another promising approach to estimate the number of infected individuals is to model the series of processes between excretion and detection with statistics distributions [59]. While our work is an important step in the direction of maximizing the potential of environmental surveillance, ultimately collaboration between wastewater engineers, pathogen specialists, and modelers will be needed to make environmental surveillance truly useful. In practice, environmental surveillance for poliovirus, SARS-CoV-

2, and other pathogens will be the most useful and easiest to interpret when done systematically, at multiple sites, and in coordination with other parallel disease surveillance approaches [18, 60–62].

Quantitative environmental surveillance has the potential to transform our analysis of outbreaks. Here, we demonstrated that including time-varying viral shedding in a model considerably changed the interpretation of a poliovirus outbreak. It is likely to do so in other cases where models are fit to wastewater data as well. To realize the full potential of environmental pathogen surveillance, we need to simultaneously advance detection technology, basic science for shedding dynamics, analytic tools and models, and the real-world implementation of environmental surveillance.

Author Contributions

AFB: conceptualization, formal analysis, methodology, software, visualization, writing – original draft, writing – review & editing. MCE: conceptualization, methodology, writing – review & editing. LSM: conceptualization, data curation, investigation, project administration, resources, writing – review & editing. MF: writing – review & editing. JSK – conceptualization, writing – review & editing. SJK: writing – review & editing. MH: investigation, methodology. YM: investigation. IG: writing – review & editing. JNSE: conceptualization, supervision, writing – review & editing.

Acknowledgments

We thank Ella Mendelson, Danit Sofer, and Merav Weil of the Central Virology Laboratory for their contributions.

Data Accessibility

The data analyzed in this manuscript are provided as supplemental material.

Ethics

Not applicable.

Funding Statement

This project was funded through Models of Infectious Disease Agent Study (MIDAS) program within the National Institute of General Medical Sciences of the National Institutes of Health (grant numbers U01GM110712 and U54GM111274), the National Science Foundation (grant numbers OCE1115881, EAR-1360330, and DMS-1853032), and the World Health Organization (grant number 353558 TSA 2014/485861-0). Funding for the Chaim Sheba Central Virology Laboratory was provided by the Israel Ministry of Health and the World Health Organization (grant number 18-TSA032).

References

[1] Munoz P, Burillo A, Bouza E. Environmental surveillance and other control measures in the prevention of nosoco-˜ mial fungal infections. Clinical Microbiology and Infection. 2006;7:38–45.

[2] Sinclair RG, Choi CY, Riley MR, Gerba CP. Pathogen Surveillance Through Monitoring of Sewer Systems; 2008.

[3] Bosch A, Guix S, Sano D, Pinto RM. New tools for the study and direct surveillance of viral pathogens in water.´ Current Opinion in Biotechnology. 2008;19(3):295–301.

[4] Aw TG, Gin KYH. Environmental surveillance and molecular characterization of human enteric viruses in tropical urban wastewaters. Journal of Applied Microbiology. 2010;109(2):716–730.

[5] Mishra A, Taneja N, Sharma M. Environmental and epidemiological surveillance of Vibrio cholerae in a choleraendemic region in India with freshwater environs. Journal of Applied Microbiology. 2012;112(1):225–237.

[6] Pannwitz G, Wolf C, Harder T. Active Surveillance for Avian Influenza Virus Infection in Wild Birds by Analysis of Avian Fecal Samples from the Environment. Journal of Wildlife Diseases. 2013;45(2):512–518.

[7] Liu J, Gratz J, Amour C, Kibiki G, Becker S, Janaki L, et al. A Laboratory-Developed TaqMan Array Card for Simultaneous Detection of 19 Enteropathogens. Journal of Clinical Microbiology. 2013;51(2):472–480.

[8] Liu J, Kabir F, Manneh J, Lertsethtakarn P, Begum S, Gratz J, et al. Development and assessment of molecular diagnostic tests for 15 enteropathogens causing childhood diarrhoea: A multicentre study. The Lancet Infectious Diseases. 2014;14(8):716–724.

[9] Manor Y, Shulman LM, Kaliner E, Hindiyeh M, Ram D, Sofer D, et al. Intensified environmental surveillance supporting the response to wild poliovirus type 1 silent circulation in Israel, 2013. Eurosurveillance. 2014;19(7):20708.

[10] Furtak V, Roivainen M, Mirochnichenko O, Zagorodnyaya T, Laassri M, Zaidi SZ, et al. Environmental surveillance of viruses by tangential flow filtration and metagenomic reconstruction. Eurosurveillance. 2016;21(15):30193.

[11] Wang T, Ma M, Anderson BD, Lednicky JA, Xia Y, Shu B, et al. Bioaerosol Sampling in Modern Agriculture: A Novel Approach for Emerging Pathogen Surveillance? Journal of Infectious Diseases. 2016;214(4):537–545.

[12] Lodder W, de Roda Husman AM. SARS-CoV-2 in wastewater: potential health risk, but also data source. The Lancet Gastroenterology & Hepatology. 2020;5(6):533–534.

[13] Bivins A, North D, Ahmad A, Ahmed W, Alm E, Been F, et al. Wastewater-Based Epidemiology: Global Collaborative to Maximize Contributions in the figureht Against COVID-19. Environmental Science & Technology. 2020;54(13):7754–7757.

[14] Kitajima M, Ahmed W, Bibby K, Carducci A, Gerba CP, Hamilton KA, et al. SARS-CoV-2 in wastewater: State of the knowledge and research needs. Science of the Total Environment. 2020;739:139076.

[15] Medema G, Been F, Heijnen L, Petterson S. Implementation of environmental surveillance for SARS-CoV-2 virus to support public health decisions: Opportunities and challenges. Current Opinion in Environmental Science & Health. 2020.

[16] Hrudey SE, Silva DS, Shelley J, Pons W, Isaac-Renton J, Chik AHS, et al. Ethics Guidance for Environmental Scientists Engaged in Surveillance of Wastewater for SARS-CoV-2. Environmental science & technology. 2021.

[17] Coffman MM, Guest JS, Wolfe MK, Naughton CC, Boehm AB, Vela JD, et al. Preventing Scientific and Ethical Misuse of Wastewater Surveillance Data. Environmental Science & Technology. 2021.

[18] Bibby K, Bivins A, Wu Z, North D. Making waves: Plausible lead time for wastewater based epidemiology as an early warning system for COVID-19. Water Research. 2021;202:117438.

[19] Anis E, Kopel E, Singer SR, Kaliner E, Moerman L, Moran-Gilad J, et al. Insidious reintroduction of wild poliovirus into Israel, 2013 Detection of wild poliovirus in Israel. Eurosurveillance. 2013;18(38).

[20] Brouwer AF, Eisenberg JNS, Pomeroy CD, Shulman LM, Hindiyeh M, Manor Y, et al. Epidemiology of the silent polio outbreak in Rahat, Israel, based on modeling of environmental surveillance data. Proceedings of the National Academy of Sciences. 2018:201808798.

[21] Berchenko Y, Manor Y, Freedman LS, Kaliner E, Grotto I, Mendelson E, et al. Estimation of polio infection prevalence from environmental surveillance data. Science Translational Medicine. 2017;9(383):eaaf6786.

[22] Kroiss SJ, Ahmadzai M, Ahmed J, Alam MM, Chabot-Couture G, Famulare M, et al. Assessing the sensitivity of the polio environmental surveillance system. PLOS ONE. 2018;13(12):e0208336.

[23] O'Reilly KM, Verity R, Durry E, Asghar H, Sharif S, Zaidi SZ, et al. Population sensitivity of acute flaccid paralysis and environmental surveillance for serotype 1 poliovirus in Pakistan: An observational study. BMC Infectious Diseases. 2018;18(1):1–10.

[24] Duintjer Tebbens RJ, Pallansch MA, Chumakov KM, Halsey NA, Hovi T, Minor PD, et al. Review and assessment of poliovirus immunity and transmission: Synthesis of knowledge gaps and identification of research needs. Risk Analysis. 2013;33(4):606–646.

[25] Famulare M, Selinger C, McCarthy KA, Eckhoff PA, Chabot-Couture G. Assessing the stability of polio eradication after the withdrawal of oral polio vaccine. PLoS Biology. 2018;16(4):1–31.

[26] Rutledge R, Cote C. Mathematics of quantitative kinetic PCR and the application of standard curves. Nucleic Acids Research. 2003;31(16):e93–e93.

[27] Hindiyeh MY, Moran-Gilad J, Manor Y, Ram D, Shulman LM, Sofer D, et al. Development and validation of a real time quantitative reverse transcription-polymerase chain reaction (QRT-PCR) assay for investigation of wild poliovirus type 1-South Asian (SOAS) strain reintroduced into Israel, 2013 to 2014. Eurosurveillance. 2014;19(7):1– 7.

[28] Shulman LM, Mendelson E, Anis E, Bassal R, Gdalevich M, Hindiyeh M, et al. Laboratory challenges in response to silent introduction and sustained transmission of wild poliovirus type 1 in Israel during 2013. The Journal of Infectious Diseases. 2014 11;(Suppl 1):304–14.

[29] Shulman LM, Manor Y, Sofer D, Handsher R, Swartz T, Delpeyroux F, et al. Neurovirulent vaccine-derived polioviruses in sewage from highly immune populations. PLOS One. 2006 12;1(1):e69.

[30] Manor Y, Blomqvist S, Sofer D, Alfandari J, Halmut T, Abramovitz B, et al. Advanced environmental surveillance and molecular analyses indicate separate importations rather than endemic circulation of wild type 1 poliovirus in Gaza district in 2002. Applied and Environmental Microbiology. 2007 9;73(18):5954–8.

[31] Yaari R, Kaliner E, Grotto I, Katriel G, Moran-Gilad J, Sofer D, et al. Modeling the spread of polio in an IPV-vaccinated population: lessons learned from the 2013 silent outbreak in southern Israel. BMC Medicine. 2016;14(1):95.

[32] Kalkowska DA, Tebbens RJD, Grotto I, Shulman LM, Anis E, Wassilak SGF, et al. Modeling Options to Manage Type 1 Wild Poliovirus Imported Into Israel in 2013. Journal of Infectious Diseases. 2015;211(11):1800–1812.

[33] Duintjer Tebbens RJ, Pallansch MA, Kalkowska DA, Wassilak SG, Cochi SL, Thompson KM. Characterizing poliovirus transmission and evolution: Insights from modeling experiences with wild and vaccine-related polioviruses. Risk Analysis. 2013;33(4):703-49.

[34] Zelner JL, Lopman BA, Hall AJ, Ballesteros S, Grenfell BT. Linking time-varying symptomatology and intensity of infectiousness to patterns of norovirus transmission. PLOS One. 2013 Jul 24;8(7):e68413.

[35] Hurtado PJ, Kirosingh AS. Generalizations of the 'Linear Chain Trick': Incorporating more flexible dwell time distributions into mean field ODE models. Journal of Mathematical Biology. 2019;79(5):1831–83.

[36] Smith H. An Introduction to Delay Differential Equations with Applications to the Life Sciences. vol. 57 of Texts in Applied Mathematics. New York, NY: Springer New York; 2011.

[37] Champredon D, Dushoff J, Earn DJD. Equivalence of the Erlang-Distributed SEIR Epidemic Model and the Renewal Equation. SIAM Journal on Applied Mathematics. 2018;78(6):3258–3278.

[38] State of Israel Ministry of Health. Vaccines for Babies and Children; 2020. https://www.health.gov.il/English/Topics/Pregnancy/Vaccination of infants/Pages/default.aspx. Accessed July 30, 2020.

[39] Soetaert K, Petzoldt T, Setzer RW. Solving Differential Equations in R: Package deSolve. Journal of Statistical Software. 2010;33(9):1–25.

[40] Luebeck G, Meza R. Bhat: General likelihood exploration; 2013. R package version 0.9-10. https://CRAN.Rproject.org/package=Bhat. Accessed February 19, 2015.

[41] Raue A, Kreutz C, Maiwald T, Bachmann J, Schilling M, Klingmuller U, et al. Structural and practical identifiability analysis of partially observed dynamical models by exploiting the profile likelihood. Bioinformatics. 2009 8;25(15):1923–9.

[42] Moran-Gilad J, Mendelson E, Burns CC, Bassal R, Gdalevich M, Sofer D, et al. Field study of fecal excretion as a decision support tool in response to silent reintroduction of wild-type poliovirus 1 into Israel. Journal of Clinical Virology. 2015;66:51–55.

[43] Piirainen L, Stenvik M, Roivainen M, Eskola J, Beuvery EC, Hovi T. Randomised, controlled trial with the trypsinmodified inactivated poliovirus vaccine: assessment of intestinal immunity with live challenge virus. Vaccine. 1999;17(9-10):1084–1090.

[44] O'Ryan M, Bandyopadhyay AS, Villena R, Espinoza M, Novoa J, Weldon WC, et al. Inactivated poliovirus vaccine given alone or in a sequential schedule with bivalent oral poliovirus vaccine in Chilean infants: a randomised, controlled, open-label, phase 4, non-inferiority study. The Lancet Infectious Diseases. 2015;15(11):1273–1282.

[45] Parker EP, Molodecky NA, Pons-Salort M, OReilly KM, Grassly NC. Impact of inactivated poliovirus vaccine on mucosal immunity: implications for the polio eradication endgame. Expert review of vaccines. 2015;14(8):1113– 1123.

[46] Shulman LM, Gavrilin E, Jorba J, Martin J, Burns CC, Manor Y, et al. Molecular epidemiology of silent introduction and sustained transmission of wild poliovirus type 1, Israel, 2013. Eurosurveillance. 2014;19(7):1–8.

[47] Tulchinsky TH, Ramlawi A, Abdeen Z, Grotto I, Flahault A. Polio lessons 2013: Israel, the West Bank, and Gaza. The Lancet. 2013 nov;382(9905):1611–1612.

[48] Mbaeyi C, Ryan MJ, Smith P, Mahamud A, Farag N, Haithami S, et al. Response to a Large Polio Outbreak in a Setting of Conflict Middle East, 20132015. Morbidity and Mortality Weekly Report. 2017;66(8):227–231.

[49] Kamadjeu R, Mahamud A, Webeck J, Baranyikwa MT, Chatterjee A, Bile YN, Birungi J, Mbaeyi C, Mulugeta A. Polio outbreak investigation and response in Somalia, 2013. The Journal of Infectious Diseases. 2014;210(Suppl 1):S181-6.

[50] Mbaeyi C, Kamadjeu R, Mahamud A, Webeck J, Ehrhardt D, Mulugeta A. Progress toward polio eradication—Somalia, 1998–2013. The Journal of infectious diseases. 2014;210(Suppl 1):S173-80.

[51] Asghar H, Diop OM, Weldegebriel G, Malik F, Shetty S, Bassioni LE, et al. Environmental surveillance for polioviruses in the global polio eradication initiative. Journal of Infectious Diseases. 2014;210(Suppl 1):S294–S303.

[52] Duintjer Tebbens RJ, Zimmermann M, Pallansch MA, Thompson KM. Insights from a Systematic Search for Information on Designs, Costs, and Effectiveness of Poliovirus Environmental Surveillance Systems. Food and Environmental Virology. 2017;9(4):361–382.

[53] Patel JC, Diop OM, Gardner T, Chavan S, Jorba J, Wassilak SG, et al. Surveillance to track progress toward polio eradicationworldwide, 2017–2018. Morbidity and Mortality Weekly Report. 2019;68(13):312.

[54] Jorgensen D, Pons-Salort M, Shaw AG, Grassly NC. The role of genetic sequencing and analysis in the polio eradication programme. Virus Evolution. 2020;6(2):veaa040.

[55] Chacon L, Morales E, Valiente C, Reyes L, Barrantes K. Wastewater-Based Epidemiology of Enteric Viruses and Surveillance of Acute Gastrointestinal Illness Outbreaks in a Resource-Limited Region. The American Journal of Tropical Medicine and Hygiene. 2021;00(00):1–9.

[56] Wolfe MK, Archana A, Catoe D, Coffman MM, Dorevich S, Graham KE, et al. Scaling of SARS-CoV-2 RNA in Settled Solids from Multiple Wastewater Treatment Plants to Compare Incidence Rates of Laboratory-Confirmed COVID-19 in Their Sewersheds. Environmental Science & Technology Letters. 2021;8(5):398–404.

[57] Lopman BA, McQuade ETR. Using viral load to model disease dynamics. Science. 2021;373(6552):280–281.

[58] Hay JA, Kennedy-Shaffer L, Kanjilal S, Lennon NJ, Gabriel SB, Lipsitch M, et al. Estimating epidemiologic dynamics from cross-sectional viral load distributions. Science. 2021;373(6552):eabh0635.

[59] Perepliotchikov Y, Ziv-Baran T, Hindiyeh M, Manor Y, Sofer D, Moran-Gilad J, et al. Inferring Numbers of Wild Poliovirus Excretors Using Quantitative Environmental Surveillance. Vaccines. 2021;9(8):870.

[60] Shulman L, Manor Y, Sofer D, Mendelson E. Bioterrorism and surveillance for infectious diseases: lessons from poliovirus and enteric virus surveillance. Journal of Bioterrorism and Biodefense. 2012;4:004.

[61] Kroiss SJ, Ahmadzai M, Ahmed J, Alam MM, Chabot-Couture G, Famulare M, et al. Assessing the sensitivity of the polio environmental surveillance system. PLOS One. 2018;13(12):e0208336.

[62] Keshaviah A, Hu XC, Henry M. Developing a Flexible National Wastewater Surveillance System for COVID-19 and Beyond. Environmental Health Perspectives. 2021;129(4):045002.

Tables

Table 1: Parameters for the polio outbreak model. Subscript i represents the subcompartment number for the distributed delays for the latent and infectious stages, and subscript j represents one of the seven wastewater sampling sites.

Parameter	Definition
β	WPV1 transmission rate, 1/d
ρ_{o1}	Ratio of OPV1 to WPV1 transmission rates
ρ_{o3}	Ratio of OPV3 to WPV1 transmission rates
ϕ	Vaccination rate, 1/d
σ_i	Latent stage transition rates, 1/d
γ_i	Infection stage transition rates, 1/d
$\alpha_{w1,j}$	Site-specific high shedding rate per wastewater volume for WPV1, copies/volume/d
$\alpha_{o1,j}$	Site-specific high shedding rate per wastewater volume for OPV1, copies/volume/d
$\alpha_{o3,j}$	Site-specific high shedding rate per wastewater volume for OPV3, copies/volume/d
λ_w	Ratio of low to high WPV1 shedding
λ_o	Ratio of low to high OPV1 & OPV3 shedding
η_j	Site-specific relative size of vaccinated but not-at-risk population
ξ_j	Rate of removal/decay of poliovirus, 1/d
τ	Copy number (i.e., concentration) threshold, copies/sample volume

Table 2: Estimated parameters for the polio outbreak model with time-varying shedding intensity

Parameter	Estimate	95% CI
WPV1 transmission rate (1/d), β	0.49	0.46–0.52
Average duration shedding (d), $\sum \gamma_i^{-1}$	29.4	27.7–31.3
Site-specific scaling parameters for WPV1, $\kappa_{w1,j}$		
Ar'ara	2.9×10^{6}	$1.6–4.9\times10^{6}$
Arad (Kseife branch)	4.7×10^{5}	$2.6–7.3\times10^{5}$
Ayalon (Lod branch)	8.1×10^{7}	$5.3–12.5\times10^{7}$
Be'er Sheva	6.0×10^{7}	$3.6–8.7\times10^{7}$
Rahat	2.2×10^{6}	$1.5–3.0\times10^{6}$
Shoket	5.3×10^{7}	$3.0–13.5\times10^{7}$
Tel Sheva	2.1×10^{6}	$1.2–3.7\times10^{6}$
Ratio of WPV1:OPV1 shedding, $\kappa_{w1,j}/\kappa_{o1,j}$	10.0	7.8–15.6
Ratio of WPV1:OPV3 shedding, $\kappa_{w1,j}/\kappa_{o3,j}$	3.7	2.7–5.1
Ratio of low to high WPV1 shedding, λ_w	7.0×10^{-3}	$4.3–12.7\times10^{-3}$
Ratio of low to high OPV1 & OPV3 shedding, λ_o	7.0×10^{-2}	$4.6–8.9\times10^{-2}$
Site-specific relative size of vaccinated but not-at-risk population, η_j		
Ayalon	8.8	4.4–19.8
Be'er Sheva	13.0	7.1–27.5
Shoket	11.8	5.5–18.8

figure captions

Figure 1: We calibrate our shedding model by specifying the number, type, order, and mean duration of the compartments, as well as the daily shedding concentrations. A shedding model specifies the latent and infectious subcompartment parameters σ_i and γ_i and the ratio of low to high shedding rates λ in our infectious disease model (table 1 and figure 2).

Figure 2: An SLIR-type model, incorporating vaccination and environmental surveillance. The model represents infection by three strains of poliovirus: WPV1 (subscript $w1$), OPV1 (subscript $o1$), and OPV3 (subscript $o3$). We assume an individual, once infected with either WPV1 or OPV1, is not affected by the other. OPV3 is modeled independently of the other two strains. The latent and infectious compartments have multiple subcompartments, as calibrated in the shedding model. Parameter definitions are given in table 1.

Figure 3: Mean expert opinion (points) and modeled simulation (lines) for the a) fraction of the infected population shedding WPV1 and b) mean fecal shedding concentration among those shedding, both as a function of time since exposure. Simulations are presented for three prior immunization states: fully susceptible (red), 3+ doses of IPV (blue), at least one dose each of IPV and OPV (yellow). Simulations are determined by specifying compartment duration and shedding concentration in the shedding model in figure 1.

Figure 4: a) Modeled fractions of the population that were infected with WPV1, OPV1, and OPV3. The ribbons give the CIs for the maximum-likelihood trajectory using likelihood-based estimates of the 95% confidence parameter region. The gray bars give the approximate periods of the bOPV vaccination campaigns. b) Epidemic trajectory of WPV1 comparing the best-fit model that incorporates a variable shedding model (solid) to the corresponding best-fit model that assumes constant shedding (dashed).

Figure 5: qRT-PCR Ct data (points) and model fits (black line) for WPV1 (left column), OPV1 (center column), and OPV3 (right column) strains in wastewater for each of the surveillance sites. The qRT-PCR data and modeled y are scaled by $\log_2$ of their respective site-specific scaling parameter κ. The ribbons give the CIs for the maximum-likelihood trajectory using likelihood-based estimates of the 95% confidence parameter region. The gray bars give the approximate periods of the bOPV campaigns.

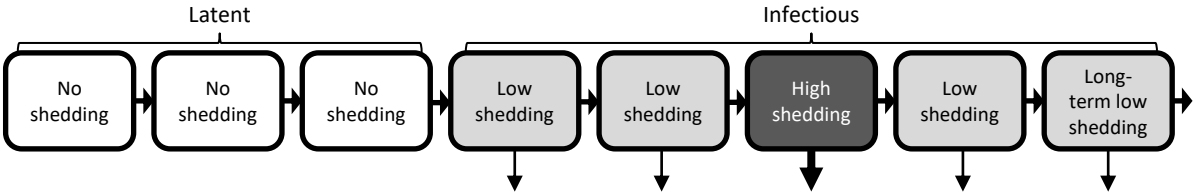
Latent
Infectious
No shedding
No shedding
No shedding
Low shedding
Low shedding
High shedding
Low shedding
Long-term low shedding

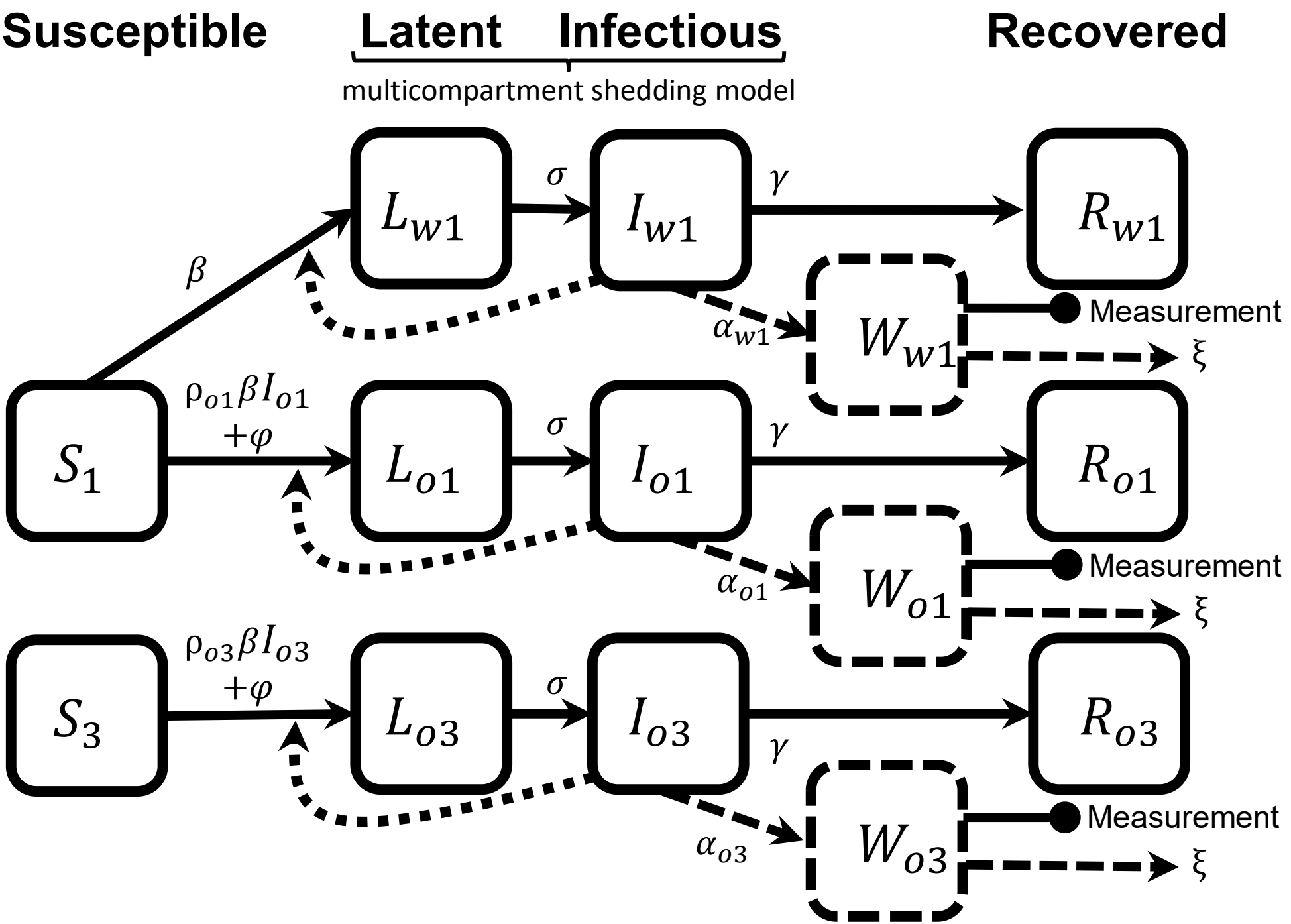
Susceptible
Latent
Infectious
Recovered
multicompartment shedding model
L_{w1}
σ
I_{w1}
γ
R_{w1}
β
α_{w1}
W_{w1}
Measurement
ξ
S_1
$\rho_{o1}\beta I_{o1}$
$+\varphi$
L_{o1}
σ
I_{o1}
γ
R_{o1}
α_{o1}
W_{o1}
Measurement
ξ
S_3
$\rho_{o3}\beta I_{o3}$
$+\varphi$
L_{o3}
σ
I_{o3}
γ
R_{o3}
α_{o3}
W_{o3}
Measurement
ξ

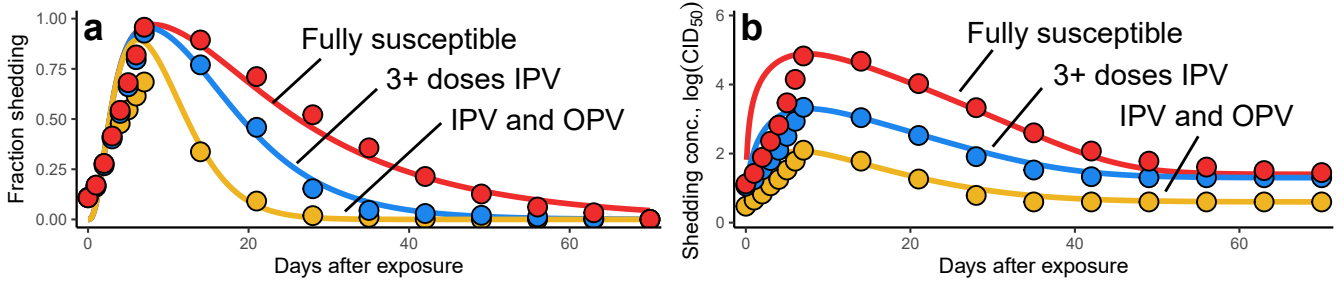
a
Fraction shedding
1.00
0.75
0.50
0.25
0.00
0
20
40
60
Days after exposure
Fully susceptible
3+ doses IPV
IPV and OPV
b
Shedding conc., log(CID50)
6
4
2
0
0
20
40
60
Days after exposure
Fully susceptible
3+ doses IPV
IPV and OPV

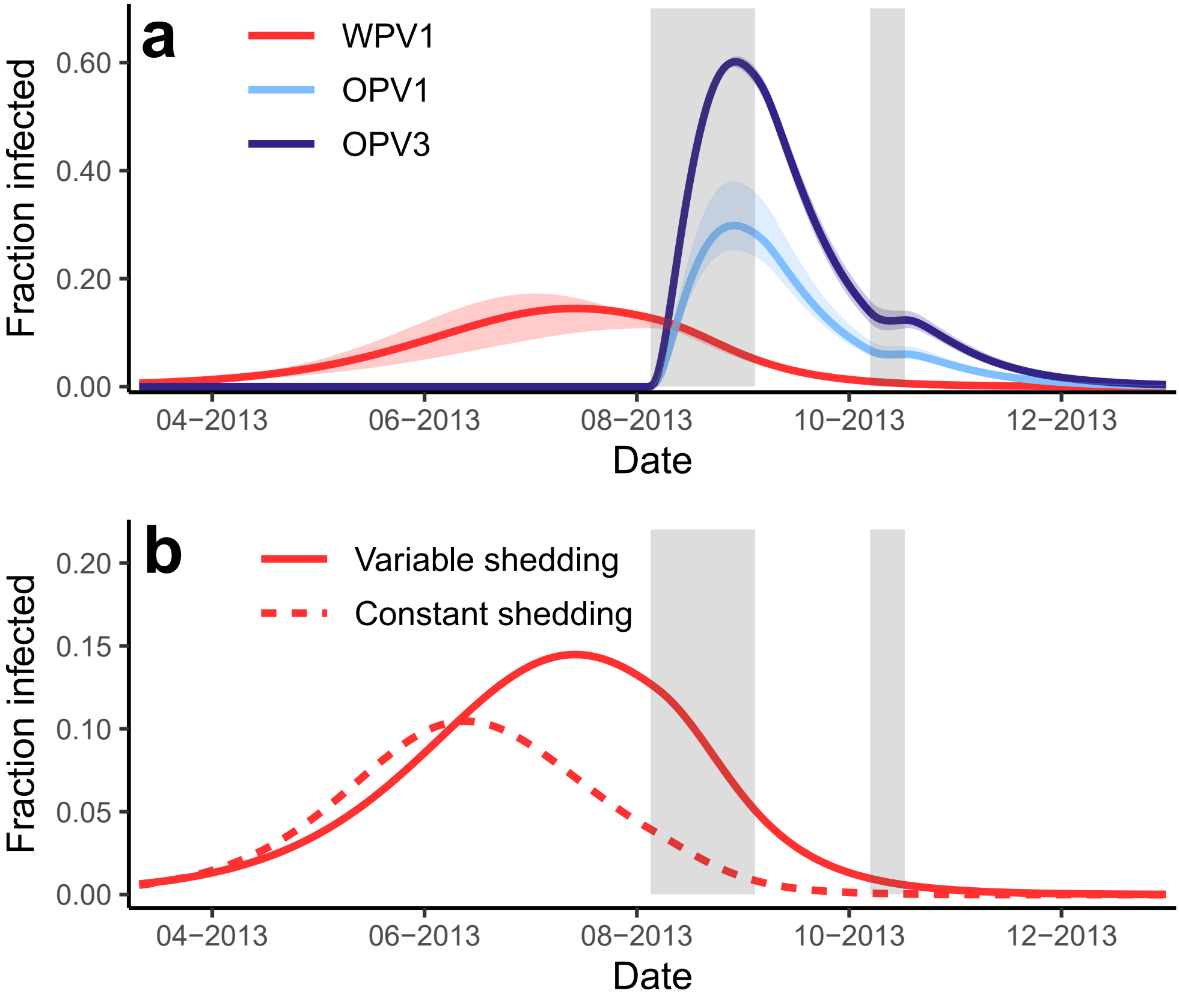
a
WPV1
OPV1
OPV3
Fraction infected
0.60
0.40
0.20
0.00
04−2013
06−2013
08−2013
10−2013
12−2013
Date
b
Variable shedding
Constant shedding
Fraction infected
0.20
0.15
0.10
0.05
0.00
04−2013
06−2013
08−2013
10−2013
12−2013
Date

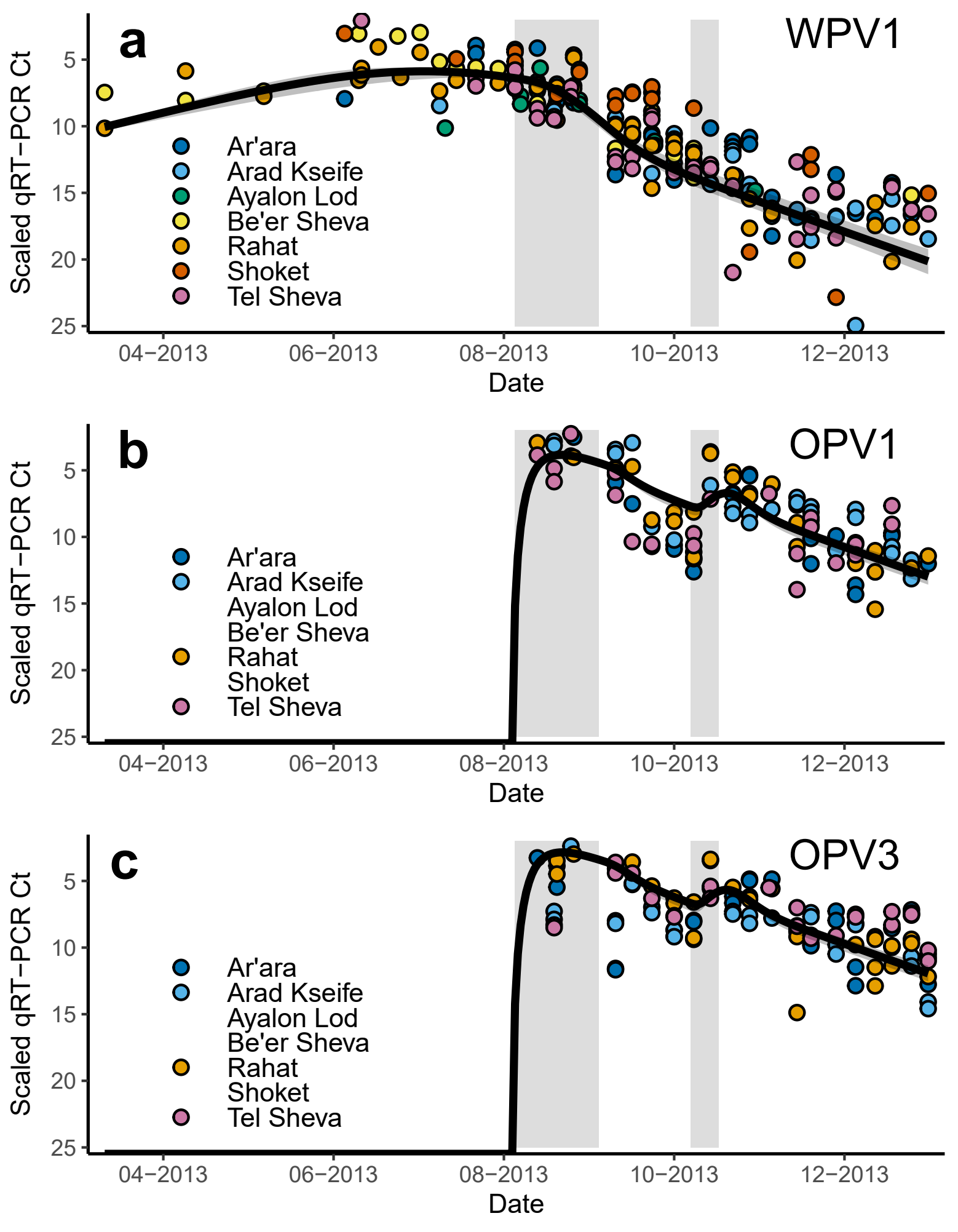
a
WPV1
Scaled qRT−PCR Ct
5
10
15
20
25
Ar'ara
Arad Kseife
Ayalon Lod
Be'er Sheva
Rahat
Shoket
Tel Sheva
04−2013
06−2013
08−2013
10−2013
12−2013
Date
b
OPV1
Scaled qRT−PCR Ct
5
10
15
20
25
Ar'ara
Arad Kseife
Ayalon Lod
Be'er Sheva
Rahat
Shoket
Tel Sheva
04−2013
06−2013
08−2013
10−2013
12−2013
Date
c
OPV3
Scaled qRT−PCR Ct
5
10
15
20
25
Ar'ara
Arad Kseife
Ayalon Lod
Be'er Sheva
Rahat
Shoket
Tel Sheva
04−2013
06−2013
08−2013
10−2013
12−2013
Date